Journal of Sound and Vibration (1998) **211**(1), 249–264

IDENTIFYING NODES AND ANTI-NODES OF COMPLEX STRUCTURES WITH VIRTUAL ELEMENTS

P. D. Cha and C. L. Dym

Department of Engineering, Harvey Mudd College, Claremont, California 91711, *U.S.A.*

AND

W. C. Wong

Pomona College, Claremont, California, U.S.A.

(*Received* 12 *August* 1996, *and in final form* 27 *October* 1997)

This paper develops an experimentally efficient procedure that allows the determination of the location of the nodes and antinodes of a complicated structure. The approach is based on attaching a virtual element, either a virtual lumped mass or a virtual grounded spring, to the system of interest and analyzing the free vibration of the assembled system as a function of the location or co-ordinate of the virtual element. When the frequency curves of the assembled system are plotted against the constraint location of the virtual element, the nodes and antinodes of the structure of interest can be extracted by examining the minima or maxima of the curves. For the virtual lumped mass, the nodes and antinodes correspond to the maxima and minima of the frequency curves, respectively, while for the virtual spring, they correspond instead to the minima and maxima of the frequency curves.

1. INTRODUCTION

Experimentalists and designers consider it important to know where the nodes of a structure are located. For example, the usefulness of accelerometers and actuators during testing and control depends on their placement. Dynamical measurements could easily be misleading or wrong if an accelerometer is inadvertently placed on or near a node. Similarly, active control systems require that actuators be accurately placed, without which their effectiveness will not be fully realized. In another engineering application, shrouds are usually added to bladed disk assemblies to increase the stiffness of the system. Thus, a shroud that is accidentally located at a node cannot achieve the objectives for which it was designed.

It is also important to be able to predict accurately the points of maximum displacement, that is, the antinodes, because one may want to incorporate additional constraints or attach vibration absorbers to the system at these points in order to minimize the response of the system. Moreover, one is able to better select space tolerances needed to ensure that a system does not come in contact with its neighbors if one knows its largest displacement. Recall that the amplitudes of free vibration mode shapes are arbitrary. Thus, the displacements at the antinodes can only be obtained up to within some arbitrary

0022–460X/98/120249 + 16 $25.00/0/sv971388

multiplicative constant. Nevertheless, knowing the location of the antinodes allows one to focus one's attention on the critical regions of the structure.

The addition of a mass to any system generally decreases the natural frequencies of the system since it leads to an increase in the overall mass of the structure. However, if the location of a virtual lumped mass, m_v, coincides with a node of the system under consideration, it will not affect the dynamics of the original system since the mass remains stationary. Thus, a plot of the natural frequencies as a function of the constraint location of the virtual lumped mass reveals the nodes of the structure as *maxima* on that plot. Interestingly, one can also extract the antinodes from the plot of ω_i versus x_v, where ω_i denotes the ith natural frequency of the assembled system and x_v represents the constraint location of the virtual lumped mass. From numerical experiments, it was observed that the antinodes of the system of interest correspond approximately to the *local minima* on the plot. The proposed identification scheme thus allows one to locate the nodes and antinodes of a system without actually examining the mode shapes.

The nodes and antinodes of a system can also be extracted by utilizing an approach based on a virtual grounded spring of stiffness k_v. It is well known that the presence of any spring generally increases the natural frequencies of the combined system. However, if the virtual grounded spring is located at a point coincident with a node of the system under consideration, it will not contribute to the stiffness of the assembled system since the spring experiences zero relative displacement. Thus, a plot of ω_i versus x_v reveals the nodes of the structure as *minima* on that plot. From such a plot one can also extract the antinodes of the system. From numerical experiments, it was observed that the antinodes correspond to the *local maxima* on that plot.

The main difference between the two approaches outlined is that the virtual lumped mass gives rise to a force that is proportional to acceleration while the virtual grounded spring gives rise to a force that is proportional to displacement. Either virtual element can be used to locate the nodes and antinodes. Experimentally and in the field, however, it is much easier to attach a lumped mass than to attach a grounded spring to a system. Thus, the virtual lumped mass approach has more intriguing implications for laboratory work, and it suggests an experimental approach to identifying nodes and antinodes of a structure.

Thus, keeping in mind the effects of adding a lumped element on the free response of a system, it is worth noting an interesting analogy between the ideas proposed in this paper and a widely used experimental practice. In particular, tracking changes in the natural frequencies of a system has long been used as a means to detect cracks in beams and to identify structural damage by virtue of a resulting change in effective stiffness [1–9]. Here, one also monitors changes in the natural frequencies that arise due to the addition of a virtual element. However, instead of analyzing the shift in the natural frequencies, one uses the maxima and minima of the frequency curves to infer the locations of the nodes and antinodes in a structure. In recent years, eigenvalue sensitivity analyses with respect to the support locations have gained considerable attention [10–13]. These analyses, however, are used primarily for the purpose of determining the optimal bracing and intermediate support locations to prohibit buckling and to reduce vibration, and not as a means to identify the locations of nodes and antinodes.

The nodes and antinodes of a system correspond to the zeros and maxima of its mode shapes. In this paper two alternative means to locate the nodes and antinodes of any dynamical system are proposed, and these methods are illustrated by examining a uniform cantilevered Euler–Bernoulli beam with various lumped attachments. The approaches outlined, however, are sufficiently general that they can be easily extended to locate the nodes and antinodes of other combined dynamical systems.

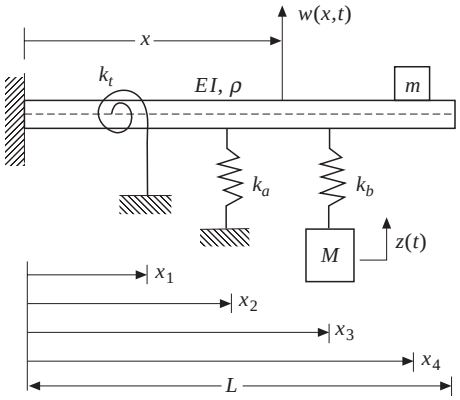

Figure 1. Original system (a uniform cantilevered Euler–Bernoulli beam to which are attached a torsional grounded spring of stiffness k_t at x_1, a translational grounded spring of stiffness k_a at x_2, a simple undamped oscillator with stiffness k_b and mass M at x_3, and a lumped mass m at x_4).

2. EQUATIONS OF MOTION

Consider a uniform cantilevered Euler–Bernoulli beam, of length L, with a set of "real" lumped attachments, including a grounded torsional spring of stiffness k_t at x_1, a grounded translational spring of stiffness k_a at x_2, a simple undamped oscillator with stiffness k_b and mass M at x_3, and a lumped mass m at x_4 (see Figure 1). This system will be referred to as the *original system*. One forms the *combined* or *assembled system* when a "virtual" element is included at x_v, where "virtual" implies that the additional element is not part of the original system of interest. The virtual element can be either a virtual lumped mass m_v (see Figure 2) or a virtual grounded spring of stiffness k_v. The formulations for each case differ slightly, as shown below.

2.1. VIRTUAL MASS APPROACH

For the system of Figure 2, the total kinetic energy of the combined or assembled system is given by

$$T = \tfrac{1}{2}\int_0^L \rho \dot{w}^2(x, t)\,\mathrm{d}x + \tfrac{1}{2}m\dot{w}^2(x_4, t) + \tfrac{1}{2}M\dot{z}^2(t) + \tfrac{1}{2}m_v\dot{w}^2(x_v, t), \tag{1}$$

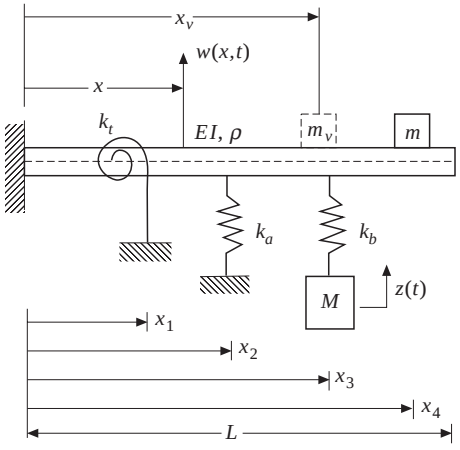

Figure 2. Combined system (original system with a virtual lumped mass, m_v, attached at x_v).

where $w(x, t)$ represents the transverse displacement at point x of the combined system, $z(t)$ is the displacement of the undamped oscillator, ρ is the linear density, and an overdot denotes the partial derivative with respect to time. The total potential energy of the system is

$$V = \tfrac{1}{2}\int_0^L EIw''^2(x, t)\,\mathrm{d}x + \tfrac{1}{2}k_t w'^2(x_1, t) + \tfrac{1}{2}k_a w^2(x_2, t) + \tfrac{1}{2}k_b[w(x_3, t) - z(t)]^2, \tag{2}$$

where E is the Young's modulus, I is the moment of inertia of the cross-section of the beam, and a prime represents the partial derivative with respect to space.

Using the Rayleigh–Ritz method [14], one writes $w(x, t)$ as

$$w(x, t) = \sum_{i=1}^{N} \phi_i(x)\eta_i(t), \tag{3}$$

where $\eta_i(t)$ is the ith normalized co-ordinate, and $\phi_i(x)$ is the ith normalized mode shape or eigenfunction of the unconstrained Euler–Bernoulli beam (or the beam without any attachments) that serves as the basis functions for this approximate solution. These basis functions are here chosen as the free vibration modes of a uniform cantilevered Euler–Bernoulli beam that satisfy the orthogonality conditions

$$\int_0^L \rho\phi_i(x)\phi_j(x)\,\mathrm{d}x = \delta_i^j \qquad \text{and} \qquad \int_0^L EI\phi_i''(x)\phi_j''(x)\,\mathrm{d}x = \lambda_i\delta_i^j. \tag{4}$$

In equation (4), δ_i^j is the Kronecker delta, $\lambda_i = (\beta_i L)^4\, EI/(\rho L^4)$ is the square of the ith natural frequency of a uniform cantilever Euler–Bernoulli beam (such that $\beta_i L$ satisfies the following transcendental equation: $\cos\beta_i L \cosh\beta_i L = -1$), and $\phi_i(x)$ is the corresponding normalized mode shape:

$$\phi_i(x) = \frac{1}{\sqrt{\rho L}}\left(\cos\beta_i x - \cosh\beta_i x + \frac{\sin\beta_i L - \sinh\beta_i L}{\cos\beta_i L + \cosh\beta_i L}(\sin\beta_i x - \sinh\beta_i x)\right). \tag{5}$$

Substituting equation (3) into equations (1) and (2) and noting the orthogonality conditions of equation (4), one obtains the following discretized total kinetic and potential energies:

$$T = \tfrac{1}{2}\sum_{i=1}^{N}\dot\eta_i^2 + \tfrac{1}{2}m\left[\sum_{i=1}^{N}\phi_i(x_4)\dot\eta_i\right]^2 + \tfrac{1}{2}M\dot z^2 + \tfrac{1}{2}m_v\left[\sum_{i=1}^{N}\phi_i(x_v)\dot\eta_i\right]^2, \tag{6}$$

$$V = \tfrac{1}{2}\sum_{i=1}^{N}\lambda_i\eta_i^2 + \tfrac{1}{2}k_t\left[\sum_{i=1}^{N}\phi_i'(x_1)\eta_i\right]^2 + \tfrac{1}{2}k_a\left[\sum_{i=1}^{N}\phi_i(x_2)\eta_i\right]^2 + \tfrac{1}{2}k_b\left[\sum_{i=1}^{N}\phi(x_3)\eta_i - z\right]^2. \tag{7}$$

Applying Lagrange's equations and assuming simple harmonic motion,

$$\eta_i(t) = \bar\eta_i\, \mathrm{e}^{\mathrm{j}\omega t}, \qquad z(t) = \bar z\, \mathrm{e}^{\mathrm{j}\omega t}, \tag{8}$$

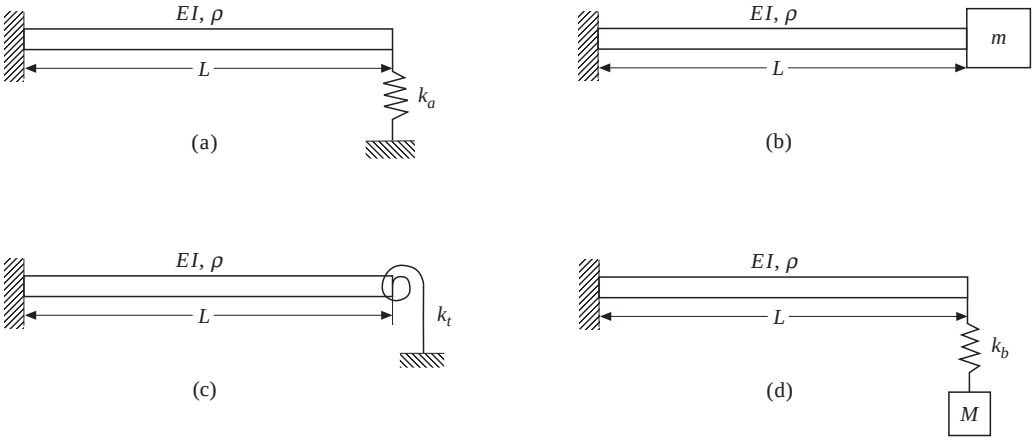

Figure 3. Cantilevered Euler–Bernoulli beam with the following lumped attachment at $x = L$: (a) a grounded translational spring k_a; (b) a lumped mass m; (c) a grounded torsional spring k_t; (d) an undamped oscillator of mass M and spring k_b.

where $\mathrm{j} = \sqrt{-1}$ and ω is the natural frequency, one obtains the eigenvalue equation for the system of Figure 2,

$$\begin{bmatrix} [\mathscr{K}] & -k_b\boldsymbol{\phi}(x_3) \\ -k_b\boldsymbol{\phi}^{\mathrm{T}}(x_3) & k_b \end{bmatrix}\begin{bmatrix} \bar{\boldsymbol{\eta}} \\ \bar{z} \end{bmatrix} = \omega^2\begin{bmatrix} [\mathscr{M}] & \mathbf{0} \\ \mathbf{0}^{\mathrm{T}} & M \end{bmatrix}\begin{bmatrix} \bar{\boldsymbol{\eta}} \\ \bar{z} \end{bmatrix}, \tag{9}$$

where the vector of normal co-ordinates $\bar{\boldsymbol{\eta}} = [\bar{\eta}_1\, \bar{\eta}_2, \ldots, \bar{\eta}_N]^{\mathrm{T}}$. The $N \times N$ matrices $[\mathscr{M}]$ and $[\mathscr{K}]$ are

$$[\mathscr{M}] = [\mathbf{I}] + m\boldsymbol{\phi}(x_4)\boldsymbol{\phi}^{\mathrm{T}}(x_4) + m_v\boldsymbol{\phi}(x_v)\boldsymbol{\phi}^{\mathrm{T}}(x_v), \tag{10}$$

$$[\mathscr{K}] = [\Lambda] + k_t\boldsymbol{\phi}'(x_1)\boldsymbol{\phi}'^{\mathrm{T}}(x_1) + k_a\boldsymbol{\phi}(x_2)\boldsymbol{\phi}^{\mathrm{T}}(x_2) + k_b\boldsymbol{\phi}(x_3)\boldsymbol{\phi}^{\mathrm{T}}(x_3). \tag{11}$$

In equations (10) and (11), $[\mathbf{I}]$ is the identity matrix, $[\boldsymbol{\Lambda}]$ is a diagonal matrix whose ith diagonal element is λ_i, and

$$\boldsymbol{\phi}(x_i) = [\phi_1(x_i)\, \phi_2(x_i), \ldots, \phi_N(x_i)]^{\mathrm{T}}, \qquad \boldsymbol{\phi}'(x_1) = [\phi_1'(x_1)\, \phi_2'(x_1), \ldots, \phi_N'(x_1)]^{\mathrm{T}}. \tag{12}$$

By inspection, since the location of the virtual lumped mass, x_v, appears in the eigenvalue equation, the natural frequencies of the combined system clearly depend on x_v.

The plots of the natural frequency against the constraint location of the virtual lumped mass reveal the nodes and antinodes of the original system. When x_v is located at a node of the original system, then $w(w_v, t) = \dot{w}(x_v, t) = 0$, and the virtual lumped mass does not contribute to the total kinetic energy of the combined system. Thus, at this location, the natural frequencies of the original and combined systems are identical. In general, the addition of a virtual lumped mass to any system decreases its natural frequencies. Consequently, the nodes of the original system correspond to the locations of the maxima of the frequency curve of the combined system when the curve is plotted as a function of the constraint location, x_v. These frequency curves also reveal the antinodes of the original system. From numerical experiments, the locations of the local minima of the natural frequency curves of the assembled system were found to correspond approximately to the locations of the antinodes of the original system (see section 3). Thus, experimentally, one can identify the nodes and antinodes of the original system by simply tracking the maxima and minima of the frequency curves when they are plotted as a function of x_v.

TABLE 1

The first four natural frequencies of Figure 3(a), *for* $k_a = 50EI/L^3$ *and* $N = 10$. *The natural frequencies are non-dimensionalized by dividing by* $\sqrt{EI/(\rho L^4)}$.

Natural frequency	Exact	Rayleigh–Ritz
1	11·5662	11·5681
2	27·0524	27·0588
3	63·4279	63·4292
4	121·7531	121·7537

TABLE 2

The first four natural frequencies of Figure 3(b), *for* $m = 2\rho L$ *and* $N = 10$. *The natural frequencies are non-dimensionalized by dividing by* $\sqrt{EI/(\rho L^4)}$.

Natural frequency	Exact	Rayleigh–Ritz
1	1·1582	1·1582
2	15·8609	15·8637
3	50·4476	50·4799
4	104·7351	104·8770

TABLE 3

The first four natural frequencies of Figure 3(c), *for* $k_t = 10EI/L$. *The natural frequencies are non-dimensionalized by dividing by* $\sqrt{EI/(\rho L^4)}$.

		(Rayleigh–Ritz)	
Natural frequency	Exact	($N = 10$)	($N = 100$)
1	5·2494	5·3738	5·2611
2	27·9705	28·7225	28·0383
3	69·7737	71·2590	69·9021
4	130·6935	132·9711	130·8831

TABLE 4

The first four natural frequencies of Figure 3(d), *for* $M = 5\rho L$, $k_b = 10EI/L^3$ *and* $N = 10$. *The natural frequencies are non-dimensionalized by dividing by* $\sqrt{EI/(\rho L^4)}$.

Natural frequency	Exact	Rayleigh–Ritz
1	0·6700	0·6700
2	7·0601	7·0604
3	22·9840	22·9841
4	62·0261	62·0261

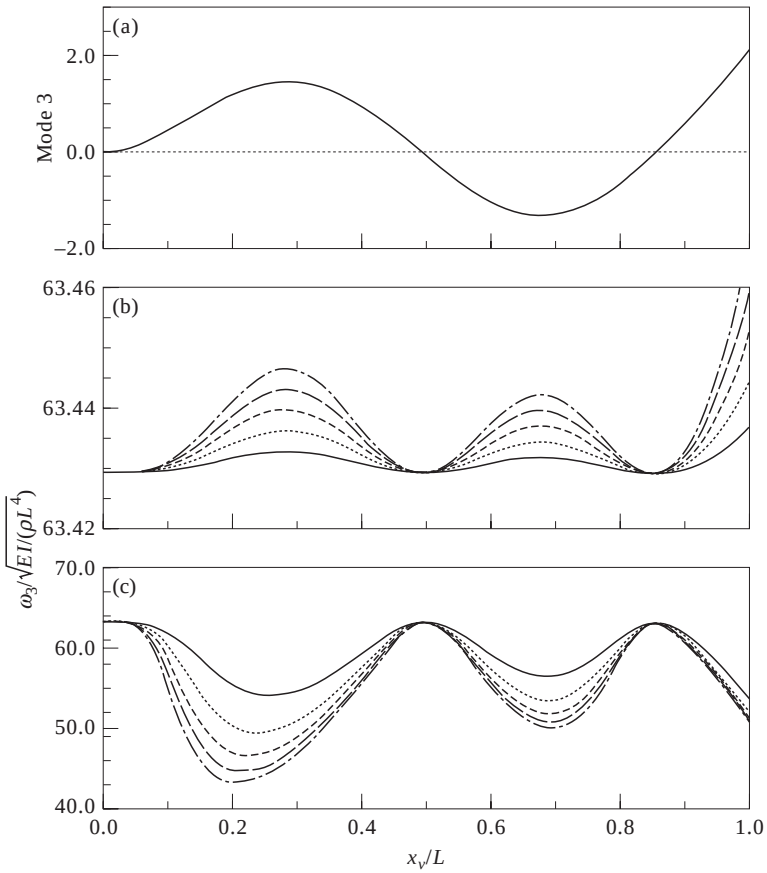

Figure 4. (a) Exact third mode shape for the system of Figure 3(a) and the corresponding frequency curves as a function of the constraint location. (b) When a virtual spring is used, the frequency curves correspond to: ——, $k_v = 0{\cdot}2$; · · · ·, 0·4; ---, 0·6; ——, 0·8; –·–, 1·0 EI/L^3. (c) When a virtual mass is used, the frequency curves correspond to: ——, $m_v = 0{\cdot}2$; · · · ·, 0·4; ---, 0·6; ——, 0·8; –·–, 1·0 ρL. The system parameters are identical to those given in Table 1.

2.2. VIRTUAL SPRING APPROACH

Using a virtual grounded spring, the total kinetic and potential energies of the combined system are given by

$$T = \tfrac{1}{2}\int_0^L \rho \dot{w}^2(x, t)\,\mathrm{d}x + \tfrac{1}{2}m\dot{w}^2(x_4, t) + \tfrac{1}{2}M\dot{z}^2(t), \tag{13}$$

$$V = \tfrac{1}{2}\int_0^L EIw''^2(x, t)\,\mathrm{d}x + \tfrac{1}{2}k_t w'^2(x_1, t) + \tfrac{1}{2}k_a w^2(x_2, t) + \tfrac{1}{2}k_b[w(x_3, t) - z(t)]^2 + \tfrac{1}{2}k_v w^2(x_v, t), \tag{14}$$

where k_v represents the stiffness of the virtual grounded spring and x_v its location. After some algebra, the frequency equation is found to be identical to equation (9). However, the $N \times N$ matrices $[\mathscr{M}]$ and $[\mathscr{K}]$ become

$$[\mathscr{M}] = [\mathbf{I}] + m\boldsymbol{\phi}(x_4)\boldsymbol{\phi}^{\mathrm{T}}(x_4), \tag{15}$$

$$[\mathscr{K}] = [\boldsymbol{\Lambda}] + k_t\boldsymbol{\phi}'(x_1)\boldsymbol{\phi}'^{\mathrm{T}}(x_1) + k_a\boldsymbol{\phi}(x_2)\boldsymbol{\phi}^{\mathrm{T}}(x_2) + k_b\boldsymbol{\phi}(x_3)\boldsymbol{\phi}^{\mathrm{T}}(x_3) + k_v\boldsymbol{\phi}(x_v)\boldsymbol{\phi}^{\mathrm{T}}(x_v). \tag{16}$$

The location of the nodes can be obtained by locating the minima of the frequency curves. Note that when x_v coincides with a node of the original system, then $w(x_v, t) = 0$. Thus, at this location, the virtual grounded spring does not deform and it does not contribute to the total potential energy of the combined system, implying that the natural frequencies of the original and combined systems must be identical. In general, the addition of a grounded spring to any system will make it stiffer, thereby increasing its natural frequencies. Hence the nodes of the ith mode shape of the original system are given by the locations of the minima of the ω_i versus x_v curve, where ω_i corresponds to the ith natural frequency of the combined system. In addition, from numerical experiments one finds that local maxima of these curves correspond approximately to the locations of the antinodes (see section 3). Thus, by tracking the locations of the minima and maxima of the frequency curves one can readily identify the nodes and antinodes of the original system.

3. RESULTS

In order to validate the proposed identification scheme one first analyzes four simple systems whose node and antinode locations can be determined exactly. The systems

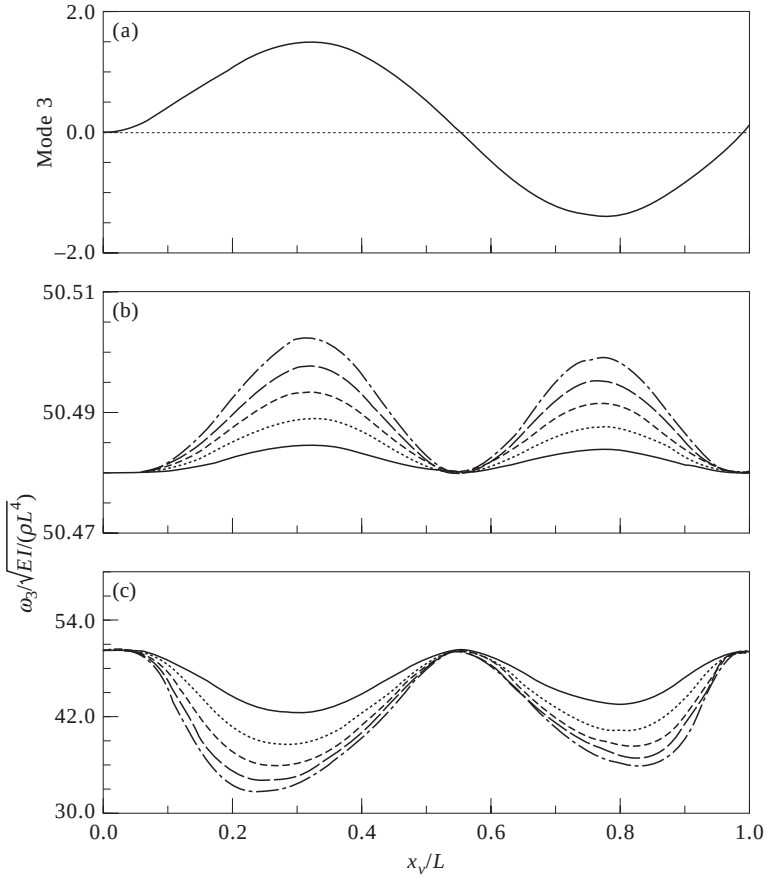

Figure 5. (a) Exact third mode shape for the system of Figure 3(b) and the corresponding frequency curves as a function of the constraint location. (b) When a virtual spring is used, the frequency curves correspond to the same values of k_v as in Figure 4. (c) When a virtual mass is used, the frequency curves correspond to the same values of m_v as in Figure 4. The system parameters are identical to those given in Table 2.

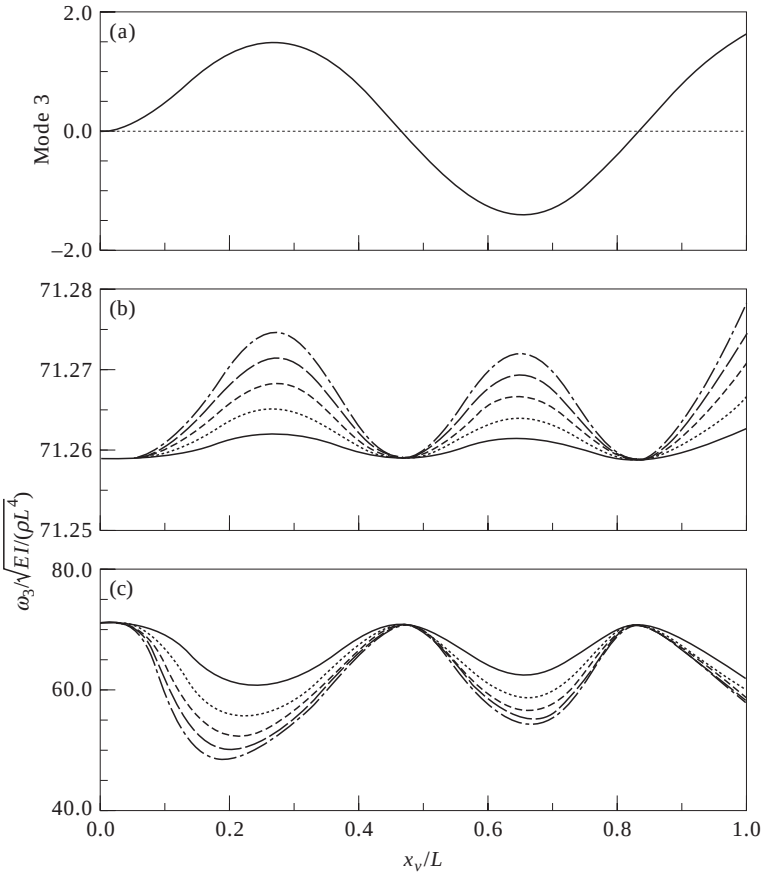

Figure 6. (a) Exact third mode shape for the system of Figure 3(c) and the corresponding frequency curves as a function of the constraint location. (b) When a virtual spring is used, the frequency curves correspond to the same values of h_v as in Figure 4. (c) When a virtual mass is used, the frequency curves correspond to the same values of m_v as in Figure 4. The system parameters are identical to those given in Table 3.

considered consist of a uniform cantilevered Euler–Bernoulli beam with a single lumped attachment at its free end. The single attachment includes a grounded translational spring, a lumped mass, a grounded torsional spring and an undamped oscillator (see Figures 3(a–d)). The transcendental equations governing the exact natural frequencies for these simple system and the corresponding expressions for the mode shapes are given in Appendix A.

Tables 1–4 compare the Rayleigh–Ritz and the exact natural frequencies for the systems of Figures 3(a–d). Note how well the approximate solution tracks the exact results for all the cases considered except when a torsional spring is attached at $x = L$. For this system, while the agreement between the two is not as good as the other systems analyzed, the approximate results are still quite accurate from an engineering perspective. The slight discrepancy between the results can be attributed to the fact that the convergence rate is very slow for the Rayleigh–Ritz approximation when a torsional spring is attached; that is, many modes, N, are needed in equation (3) in order for the approximate result to converge to the exact solution. For $N = 100$, the agreement between the Rayleigh–Ritz and exact natural frequencies becomes quite good, as shown in Table 3.

Figures 4–7 illustrate the exact mode shape of the original system and the natural frequency curves of the combined system as a function of the constraint location for the systems of Figures 3(a–d) respectively. For brevity, only the third mode shape and $\omega_3/\sqrt{EI/(\rho L^4)}$ (normalized third natural frequency) versus x_v/L for each system is shown. The sensitivity of the identification scheme to the virtual grounded spring stiffness and the virtual lumped mass is also examined by varying k_v and m_v. Based on the results of Figures 4–7, one observes the following:

When a virtual lumped mass is used, the locations of the maxima of the natural frequency curves of the combined system correspond to the nodes of the original system, and they are independent of m_v. The locations of the local minima of the frequency curves vary with m_v. The magnitude of m_v affects the location of the first local minimum the most, other local minima shift sideways only slightly in comparison. As m_v decreases, the local minima converge to the antinodes of the original system. Finally, as m_v increases, the entire frequency curve shifts downward because the mass of the combined system becomes larger.

When a virtual grounded spring is used, the locations of the minima of the natural frequency curves of the assembled system correspond to the nodes of the original system, and they are independent of the stiffness of the virtual spring. The locations of the local maxima of the natural frequency curves remain nearly constant as k_v varies. Finally, as

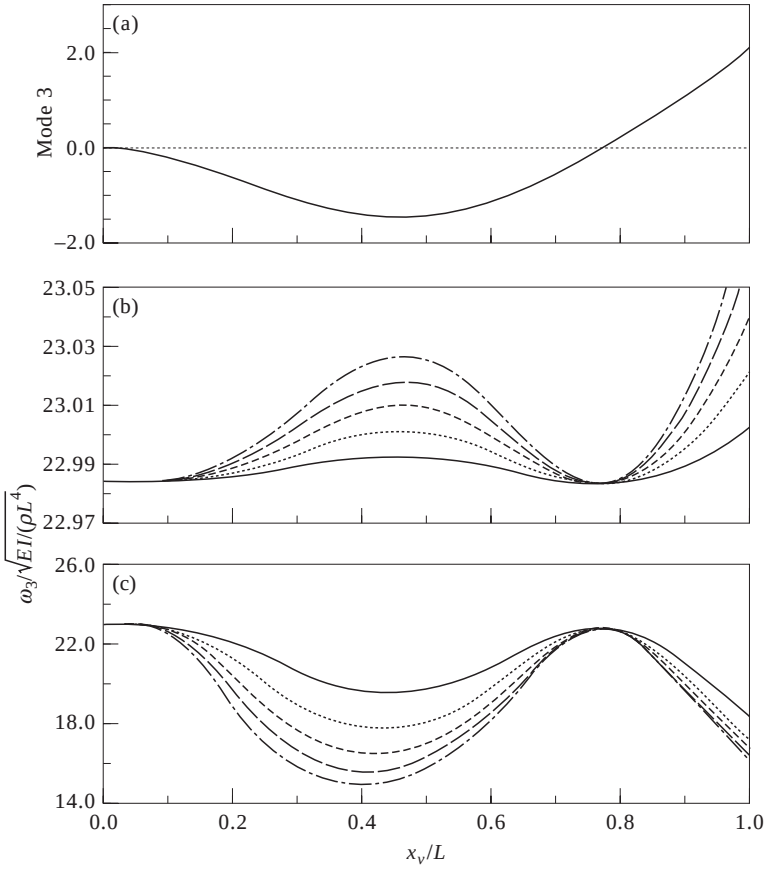

Figure 7. (a) Exact third mode shape for the system of Figure 3(d) and the corresponding frequency curves as a function of the constraint location. (b) When a virtual spring is used, the frequency curves correspond to the same values of k_v as in Figure 4. (c) When a virtual mass is used, the frequency curves correspond to the same values of m_v as in Figure 4. The system parameters are identical to those given in Table 4.

TABLE 5

Location of nodes and antinodes of Figure 3(a), *for* $k_a = 50EI/L^3$ *and* $N = 10$, *determined exactly and by using the virtual grounded spring approach. The subscripts n and an denote the* "*node*" *and* "*antinode*", *respectively, while the superscript e and vs correspond to* "*exact*" *and* "*virtual spring*". *Above results are obtained by setting* $k_v = 1EI/L^3$, *where* k_v *represents the stiffness of the virtual grounded spring, and* $N = 10$.

Mode number	x_n^e	x_n^{vs}	x_{an}^e	x_{an}^{vs}
2	0·715L	0·715L	0·427L	0·427L
3	0·497L	0·497L	0·287L	0·287L
	0·856L	0·856L	0·683L	0·683L
4	0·357L	0·357L	0·207L	0·207L
	0·642L	0·642L	0·499L	0·499L
	0·902L	0·902L	0·777L	0·777L

k_v increases, the entire frequency curves shift upwards because the overall stiffness of the assembled system becomes larger.

The frequency curves are more sensitive to the presence of a virtual mass than a virtual spring. For $m_v = 1\rho L$ and $k_v = 1EI/L^3$, the frequency ranges differ substantially (note the scaling of the abscissa of the plots) as x_v/L goes from 0 to 1. This is advantageous because it implies that one can track the frequency changes easier with a virtual lumped mass, which also happens to be the easier of the two elements to attach to the system of interest experimentally.

The nodes of a structure can be located by using either a virtual lumped mass or a virtual grounded spring approach. Experimentally, since it is much easier to attach a lumped mass to a structure than to attach a grounded spring, the virtual mass approach may prove more feasible in application. From numerical experiments, one observed that when a virtual lumped mass is used, the location of the minima of the frequency curves, which correspond to the antinodes, depend on the magnitude of m_v and they tend to shift sideways as m_v varies. One suspects that because m_v gives rise to a force that is proportional to acceleration (hence to ω^2 since the free vibration motion is harmonic), m_v affects the natural frequency curves in an odd and interesting way. Nevertheless, as m_v becomes smaller, the location of the local minima of the frequency curves of the combined system approach those of the antinodes of the original system. Keeping this in mind, the authors recommend that when using this approach experimentally to locate the antinodes of a system, one needs

TABLE 6

Location of nodes and antinodes of Figure 3(b), *for* $m = 2\rho L$ *and* $N = 10$, *determined exactly and by using the virtual grounded spring approach. The subscripts n and an denote the* "*node*" *and* "*antinode*", *respectively, while the superscript e and vs correspond to* "*exact*" *and* "*virtual spring*". *Above results are obtained by setting* $k_v = 1EI/L^3$, *where* k_v *represents the stiffness of the virtual grounded spring.*

Mode number	x_n^e	x_n^{vs}	x_{an}^e	x_{an}^{vs}
2	0·973L	0·973L	0·570L	0·570L
3	0·555L	0·555L	0·322L	0·322L
	0·991L	0·990L	0·774L	0·773L
4	0·385L	0·385L	0·223L	0·224L
	0·691L	0·690L	0·538L	0·538L
	0·995L	0·995L	0·844L	0·844L

TABLE 7

Location of nodes and antinodes of Figure 3(c), *for* $k_t = 10EI/L$ *and* $N = 10$, *determined exactly and by using the virtual grounded spring approach. The subscripts n and an denote the "node" and "antinode", respectively, while the superscript e and vs correspond to "exact" and "virtual spring". Above results are obtained by setting* $k_v = 1EI/L^3$, *where* k_v *represents the stiffness of the virtual grounded spring.*

Mode number	x_n^e	x_n^{vs}	x_{an}^e	x_{an}^{vs}
2	$0{\cdot}736L$	$0{\cdot}730L$	$0{\cdot}423L$	$0{\cdot}430L$
3	$0{\cdot}472L$	$0{\cdot}467L$	$0{\cdot}271L$	$0{\cdot}274L$
	$0{\cdot}837L$	$0{\cdot}831L$	$0{\cdot}649L$	$0{\cdot}657L$
4	$0{\cdot}345L$	$0{\cdot}342L$	$0{\cdot}197L$	$0{\cdot}200L$
	$0{\cdot}619L$	$0{\cdot}613L$	$0{\cdot}477L$	$0{\cdot}481L$
	$0{\cdot}885L$	$0{\cdot}879L$	$0{\cdot}749L$	$0{\cdot}754L$

to select a virtual lumped mass that is as small as possible to ensure that the minima of the frequency curves correspond to the antinodes, yet large enough to allow one to detect changes in the natural frequencies of the combined system.

Analytically, however, the locations of the antinodes can be best located using a virtual grounded spring scheme, since the maxima of the frequency curves are nearly invariant of k_v. Thus, in the subsequent analyses, one uses a virtual grounded spring approach to locate the antinodes of a structure. Shown in Tables 5–8 are the nodes and antinodes of the original system, obtained exactly (by solving for the zeros and the maxima of the mode shapes) and by using the virtual grounded spring approach (by locating the minima and local maxima of the frequency curves). For all the systems considered in Figures 3(a–d), there is no node for the first mode shape. For the system of Figure 3(d), there is also no node for the second mode shape. Moreover, since the cantilevered beam has its free end at $x = L$, that point is not considered as an antinode. From Tables 5–8, note how well the virtual grounded spring approach locates the nodes and antinodes.

Numerically, the accuracy of the proposed identification scheme is limited by the number of modes, N, used in the Rayleigh–Ritz approximation and by the increment of x_v used to generate the natural frequency plots. To ensure sufficient accuracy, one can take N to be very large and make the increment of x_v very small; however, one increases the computational time and cost substantially. Experimentally, the accuracy of the approach depends on the increment of x_v used, which in turn depends on the mode shapes of interest. Since one is primarily interested in the lower vibrational modes for most engineering applications, one expects that the proposed identification scheme can be used efficiently

TABLE 8

Location of nodes and antinodes of Figure 3(d), *for* $M = 5\rho L$, $k_b = 10EI/L^3$ *and* $N = 10$, *determined exactly and by using the virtual grounded spring approach. The subscripts n and an denote the "node" and "antinode", respectively, while the superscript e and vs correspond to "exact" and "virtual spring". Above results are obtained by setting* $k_v = 1EI/L^3$, *where* k_v *represents the stiffness of the virtual grounded spring.*

Mode number	x_n^e	x_n^{vs}	x_{an}^e	x_{an}^{vs}
3	$0{\cdot}768L$	$0{\cdot}768L$	$0{\cdot}461L$	$0{\cdot}461L$
4	$0{\cdot}502L$	$0{\cdot}502L$	$0{\cdot}290L$	$0{\cdot}290L$
	$0{\cdot}865L$	$0{\cdot}865L$	$0{\cdot}691L$	$0{\cdot}690L$

TABLE 9

The first four natural frequencies of Figure 2, *for* $k_a = 10EI/L^3$, $x_2 = 0{\cdot}35L$; $m = 2\rho L$, $x_4 = 0{\cdot}9L$; $k_t = 1EI/L$, $x_1 = 0{\cdot}25L$; $k_b = 5EI/L^3$, $M = 3\rho L$, $x_3 = 0{\cdot}7L$ *and* $N = 10$. *The natural frequencies are non-dimensionalized by dividing by* $\sqrt{EI/(\rho L^4)}$.

Natural frequency	Finite elements	Rayleigh–Ritz
1	0·9675	0·9678
2	1·9437	1·9440
3	20·2993	20·3040
4	60·6866	60·6899

TABLE 10

Location of nodes and antinodes of Figure 2, *for* $k_a = 10EI/L^3$, $x_2 = 0{\cdot}35L$; $m = 2\rho L$, $x_4 = 0{\cdot}9L$; $k_t = 1EI/L$, $x_1 = 0{\cdot}25L$; $k_b = 5EI/L^3$, $M = 3\rho L$, $x_3 = 0{\cdot}7/L$ *and* $N = 10$, *determined exactly and by using the virtual grounded spring approach. The subscripts n and an denote the "node" and "antinode", respectively, while the superscript fe and vs correspond to "finite elements" and "virtual spring". Above results are obtained by setting* $k_v = 1EI/L^3$, *where* k_v *represents the stiffness of the virtual grounded spring.*

Mode number	x_n^{fe}	x_n^{vs}	x_{an}^{fe}	x_{an}^{vs}
3	$0{\cdot}883L$	$0{\cdot}883L$	$0{\cdot}521L$	$0{\cdot}521L$
4	$0{\cdot}509L$	$0{\cdot}509L$	$0{\cdot}294L$	$0{\cdot}293L$
	$0{\cdot}896L$	$0{\cdot}896L$	$0{\cdot}705L$	$0{\cdot}706L$

to reveal the approximate locations of the nodes and antinodes of a structure with a limited number of data points.

Having validated the proposed identification scheme on simple systems, the authors proceeded to analyze the complicated system of Figure 1. Table 9 compares the Rayleigh–Ritz and the finite element natural frequencies, and Table 10 shows the nodes and antinodes obtained by using the virtual grounded spring approach (for the set of system parameters chosen, there is no node in the first and second mode shapes). For comparison, the nodes and antinodes are also obtained via finite elements by locating the zeros and the maxima of the mode shapes. Note the excellent agreement between the results. Figure 8 illustrates that the nodes and antinodes of Figure 1 correspond to the local minima and local maxima of the frequency curves of the combined system when they are plotted against the constraint location.

4. CONCLUSIONS

The authors have demonstrated an expermentally efficient procedure that allows the determination of the location of the nodes and antinodes of a complicated structure. The approach involves attaching a virtual lumped mass or a virtual grounded spring to the system of interest and analyzing the free vibration of the assembled system using the location or co-ordinate of the virtual element as a prime parameter. This frequency approach was shown to be useful for identifying the locations of both the nodes and antinodes.

Finally, one anticipates that the proposed methods of locating nodes and antinodes can be extended to surface structures such as plates and shells, and accordingly some

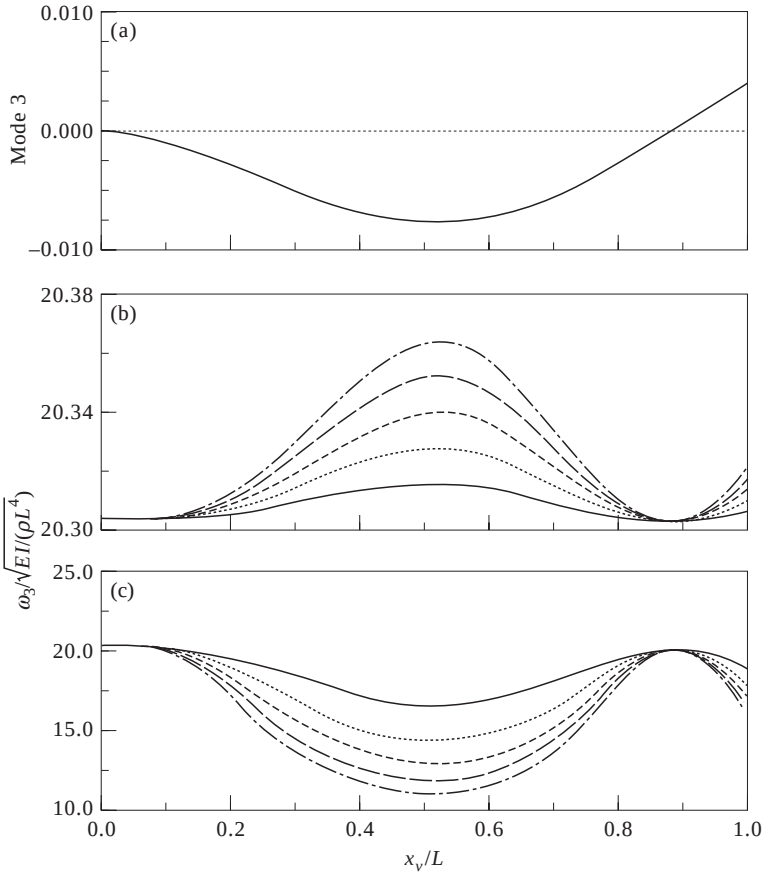

Figure 8. (a) Exact third mode shape for the system of Figure 1 and the corresponding frequency curves as a function of the constraint location. (b) When a virtual spring is used, the frequency curves correspond to the same values of k_v as in Figure 4. (c) When a virtual mass is used, the frequency curves correspond to the same values of m_v as in Figure 4. The system parameters are identical to those given in Table 9.

exploratory studies have been initiated. The authors also plan to initiate a companion study designed to determine *experimentally* the nodes and antinodes of a complex structure without having determined its mode shapes in advance. Such a study could prove quite useful, since knowing the locations of the nodes, antinodes and the component modes, one can predict the mode shapes with greater accuracy.

REFERENCES

1. A. Morassi 1993 *Journal of Engineering Mechanics* **119**, 1798–1803. Crack-induced changes in eigenparameters of beam structures.
2. W. M. Ostachowicz and M. Krawczuk 1991 *Journal of Sound and Vibration* **150**, 191–201. Analysis of the effect of cracks on the natural frequencies of a cantilever beam.
3. J. N. Sundermeyer and R. L. Weaver 1995 *Journal of Sound and Vibration* **183**, 857–871. On crack identification and characterization in a beam by non-linear vibration analysis.
4. A. K. Panday and M. Biswas 1994 *Journal of Sound and Vibration* **169**, 3–17. Damage detection in structures using changes in flexibility.
5. G. L. Qian, S. N. Gu and J. S. Jiang 1990 *Journal of Sound and Vibration* **138**, 233–243. The dynamic behaviour and crack detection of a beam with a crack.

6. R. Y. Liang, J. Hu and F. Choy 1992 *Journal of Engineering Mechanics* **118**, 384–396. Theoretical study of crack-induced eigenfrequency changes on beam structures.
7. G. Hearn and R. B. Testa 1991 *Journal of Engineering Mechanics* **117**, 3042–3063. Modal analysis for damage detection in structures.
8. P. F. Rizos and N. Aspragathos 1990 *Journal of Sound and Vibration* **138**, 381–388. Identification of crack location and magnitude in a cantilever beam from the vibration modes.
9. M. F. Yuen 1985 *Journal of Sound and Vibration* **103**, 301–310. A numerical study of the eigenparameters of a damaged cantilever.
10. B. P. Wang 1993 *AIAA Journal* **31**, 791–793. Eigenvalue sensitivity with respect to location of internal stiffness and mass attachments.
11. C. M. Wang, K. K. Ang and L. Wang 1995 *Structural Optimization* **9**, 12–17. Optimization of bracing and internal support locations for beams against lateral buckling.
12. Z. S. Liu, H. C. Hu and D. J. Wang 1996 *AIAA Journal* **34**, 864–866. A new method for eigenvalue sensitivity with respect to support locations.
13. Z. S. Liu and C. D. Mote, Jr. 1997 *Journal of Sound and Vibration* **204**, 623–630. A new discrete approach to eigenvalue sensitivity with respect to constraint locations.
14. C. L. Dym and I. H. Shames 1973 *Solid Mechanics*: *A Variational Approach*. New York: McGraw-Hill.

APPENDIX A: NATURAL FREQUENCIES AND MODES

A.1. CANTILEVERED BEAM WITH TRANSLATIONAL GROUNDED SPRING

The frequency equation of Figure 3(a) is given by

$$f(y) = ad - bc = 0, \qquad y = \beta L,$$

where $(\beta L)^2$ denotes the dimensionless natural frequency and

$$a = \cos y + \cosh y, \qquad b = \sin y + \sinh y,$$
$$c = y^3(\sin y - \sinh y) - \hat{k}_a(\cos y - \cosh y),$$
$$d = -y^3(\cos y + \cosh y) - \hat{k}_a(\sin y - \sinh y)$$

and $\hat{k}_a = k_a/(EI/L^3)$. The corresponding mode shape is

$$u(x) = A\left(\cos \beta x - \cosh \beta x - \frac{\cos \beta L + \cosh \beta L}{\sin \beta L + \sinh \beta L}(\sin \beta x - \sinh \beta x)\right),$$

where A is an arbitrary constant.

A.2. CANTILEVERED BEAM WITH LUMPED MASS

The frequency equation of Figure 3(b) is given by

$$f(y) = ad - bc = 0, \qquad y = \beta L,$$

where $(\beta L)^2$ denotes the dimensionless natural frequency and

$$a = \sin y - \sinh y + \hat{m}y(\cos y - \cosh y),$$
$$b = -\cos y - \cosh y + \hat{m}y(\sin y - \sinh y),$$
$$c = \cos y + \cosh y, \qquad d = \sin y + \sinh y$$

and $\hat{m} = m/(\rho L)$. The corresponding mode shape is

$$u(x) = A\left(\cos \beta x - \cosh \beta x - \frac{\cos \beta L + \cosh \beta L}{\sin \beta L + \sinh \beta L}(\sin \beta x - \sinh \beta x)\right),$$

where A is an arbitrary constant.

A.3. CANTILEVERED BEAM WITH GROUNDED TORSIONAL SPRING

The frequency equation of Figure 3(c) is given by

$$f(y) = ad - bc = 0, \qquad y = \beta L,$$

where $(\beta L)^2$ denotes the dimensionless natural frequency and

$$a = y(\cos y + \cosh y) + \hat{k}_t(\sin y + \sinh y),$$
$$b = y(\sin y + \sinh y) + \hat{k}_t(\cosh y - \cos y),$$
$$c = \sin y - \sinh y, \qquad d = -\cos y - \cosh y$$

and $\hat{k}_t = k_t/(EI/L)$. The corresponding mode shape is

$$u(x) = A\left(\cos \beta x - \cosh \beta x - \frac{\cos \beta L + \cosh \beta L}{\sin \beta L + \sinh \beta L}(\sin \beta x - \sinh \beta x)\right),$$

where A is an arbitrary constant.

A.4. CANTILEVERED BEAM WITH SPRING–MASS OSCILLATOR

The frequency equation of Figure 3(d) is given by

$$f(y) = \det [\mathbf{B}] = 0, \qquad y = \beta L,$$

where $(\beta L)^2$ denotes the dimensionless natural frequency, and the elements of the 3×3 matrix [**B**] are given by

$$b_{11} = \cos y + \cosh y, \qquad b_{12} = \sin y + \sinh y, \qquad b_{13} = 0,$$
$$b_{21} = y^3(\sin y - \sinh y) - \hat{k}_b(\cos y - \cosh y),$$
$$b_{22} = y^3(-\cos y - \cosh y) - \hat{k}_b(\sin y - \sinh y), \qquad b_{23} = \hat{k}_b,$$
$$b_{31} = \hat{k}_b(\cos y - \cosh y), \qquad b_{32} = \hat{k}_b(\sin y - \sinh y), \qquad b_{33} = y^4\hat{M} - \hat{k}_b$$

and $\hat{k}_b = k_b/(EI/L^3)$ and $\hat{M} = M/(\rho L)$. The corresponding mode shape is

$$u(x) = A\left(\cos \beta x - \cosh \beta x - \frac{\cos \beta L + \cosh \beta L}{\sin \beta L + \sinh \beta L}(\sin \beta x - \sinh \beta x)\right),$$

where A is an arbitrary constant.